Received: 23 May 2024 | Revised: 12 September 2024 | Accepted: 13 September 2024

DOI: 10.1002/eqe.4242

RESEARCH ARTICLE

WILEY

Fragility functions for low-damage post-tensioned timber frames

Michele Matteoni[1] | **Jonathan Ciurlanti**[2] | **Simona Bianchi**[3] | **Stefano Pampanin**[1]

[1]Department of Structural and Geotechnical Engineering, Sapienza University of Rome, Rome, Italy

[2]Arup Netherlands, Amsterdam, The Netherlands

[3]Department of Architectural Engineering and Technology, Delft University of Technology, Delft, The Netherlands

Correspondence
Michele Matteoni, Department of Structural and Geotechnical Engineering, Sapienza University of Rome, Via Eudossiana 18, 00184 Rome, Italy.
Email: michele.matteoni@uniroma1.it

Funding information
National Research Centre CN1 on "High-Performance Computing, Big Data and Quantum Computing"—Spoke 5 - Environment and Natural Disaster: Framework and methodologies for impact evaluation and risk mitigation, Grant/Award Number: B83C22003480006; ENHANCE project, Grant/Award Number: B89J21022640002; Horizon Europe Research & Innovation Programme, Grant/Award Number: 101123467

Abstract

The growing concern over environmental impact and the significant improvement in the quality of engineered wood products have led to the rapid growth of the timber building industry in the last decades. Although traditional, yet recent, mass timber structural systems, such as cross-laminated timber walls, can provide satisfactory seismic performance during earthquakes in terms of life-safety, the crucial need for more resilient timber buildings has prompted the development of low-damage high-performance self-centring and dissipative solutions based on unbonded post-tensioned hybrid connections, referred to as Pres-Lam technology. The flexibility of design and construction speed, combined with the enhanced seismic performance, create a unique potential towards an earthquake-proof sustainable building system. Despite the growing popularity of the technology, a comprehensive framework for the fragility analysis, to be used in risk and loss modelling applications, has not yet been developed for both component and building levels.

This article aims to develop a framework for assessing the fragility curves of moment-resisting Pres-Lam frame systems, at both structural system and connection levels, by using and comparing different approaches that involve nonlinear static (pushover) and time history dynamic analyses. A Python-based parametric workflow was developed to evaluate fragility curves for a wide range of case-study buildings. Particularly, three distinct structures were selected, and their fragility curves were evaluated utilizing alternative methodologies at a building structural-system level. Finally, fragility models were fitted for individual structural connections using the results of time-history analyses. These models are intended for use in a component-based loss assessment.

KEYWORDS
controlled rocking and dissipative connections, fragility curves, low-damage, parametric analysis, post-tensioned timber, Pres-Lam

1 | INTRODUCTION

Despite representing slightly less than 9% of total natural disasters recorded in between 2000 and 2019, earthquakes accounted for 58% of the disaster-related 1.23 million lives lost.[1] To reduce the fatalities, modern building codes target Life-Safety objectives, thus inherently accepting damage to both the structural skeleton and the non-structural envelope/components. In fact, according to current seismic design philosophies, structural systems are designed to concentrate damage in specific regions, which are designed to deform plastically and provide global structural ductility. While this approach has been effective in reducing casualties, it often results in significant damage to structural components, which can be expensive to repair and may ultimately require demolition.[2] Furthermore, the performance of non-structural components is typically not considered in a life-safety-targeted design approach, despite being a significant source of economic losses.[3] Earthquake-induced damage to the building envelope not only results in greater expenses and thus higher socioeconomic impact, but also leads to a significant and often underestimated environmental impact (e.g., in terms of CO_2 emissions and direct energy consumption) due to the need for component repairs (e.g.,[4–6]). Global efforts to achieve carbon neutrality in the coming decades have prompted nations worldwide to rethink the way we build our cities. It is worth noting that in the EU alone, the building industry accounts for 39% of carbon dioxide (CO_2) emissions.[7] In seismic-prone areas, this need is particularly pressing, as code-conforming building practices, while crucial for ensuring human safety during earthquakes, can result in high economic losses and contribute significantly to carbon emissions. This highlights the urgent need for sustainable building practices that balance safety, economic, and environmental considerations.

For this reason, engineered wood products are experiencing a significant increase in popularity, partly due to the versatility in design and speed of construction. Particularly, cross-laminated timber (CLT) wall systems have shown a good ability to withstand earthquake actions (e.g.,[8,9]), despite still experiencing structural damage (e.g.,[10–12]) and, especially when the sliding mechanism is predominant, residual displacements.

Growing concerns about earthquake-induced damage prompted the development of the post-tensioning timber (Pres-Lam) technology in the past 20 years,[13–15] which employs mass timber products to create a low-damage seismic structural system (Figure 1). The technology is based on the evolution and adaptation to timber of the hybrid solution for frames and walls developed since the PREcast Seismic Structural System (PRESSS) program in the 1990s,[2,16–20] which utilized post-tensioned unbonded tendons and damping devices to dissipate energy during seismic events and minimize residual deformations. Connections are designed to endure substantial deformation while suffering little to no damage thanks to a rocking mechanism. Furthermore, external Plug and Play damping devices[14,21,22] can replace internal mild steel bars, making it easier to access and repair these sacrificial components. This solution allows for a desirable ductile behaviour without incurring costly repairs. The success and high potential of the PRESSS technology led to the creation of similar systems using different materials, such as timber (the above-mentioned Pres-Lam system) and steel.[23] While the Pres-Lam technology and similar low-damage structural systems have shown outstanding performance in reducing socio-economic losses from earthquake-induced damage, it is crucial to also incorporate low-damage non-structural elements to further limit the overall impact (social, economic, environmental) of such events.[4,24–28]

The Pres-Lam system is therefore able to combine the advantages of timber buildings and low-damage technologies thus providing modularity and sustainability while limiting the component post-earthquake damage and providing re-centring capabilities. The performance of this solution was extensivity proven by experimental testing (e.g.,[14,29–35]) that highlighted the capacity of the connection to withstand a large number of cycles without degrading. Furthermore, this technology has proved highly versatile by offering a wide variety of solutions, such as single and coupled walls, which can be combined with post-tensioned frames to provide a robust and complete structural system (e.g.,[36]). Moreover, the

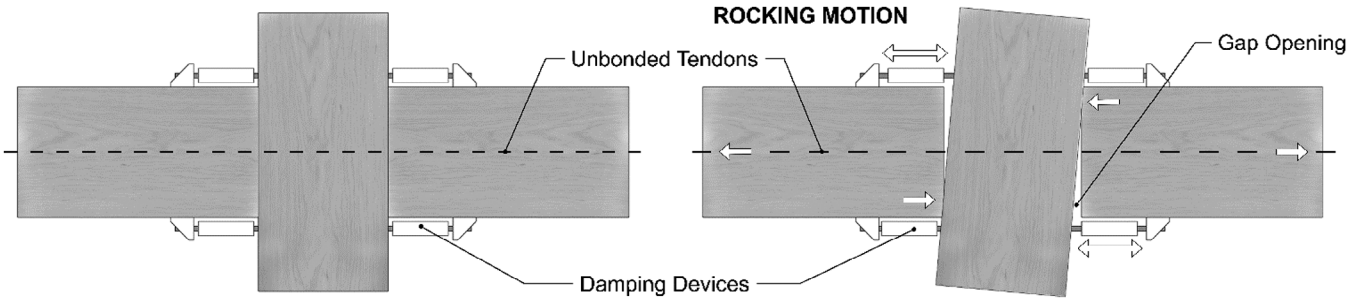

FIGURE 1 Hybrid post-tensioned dissipative connection for timber elements.

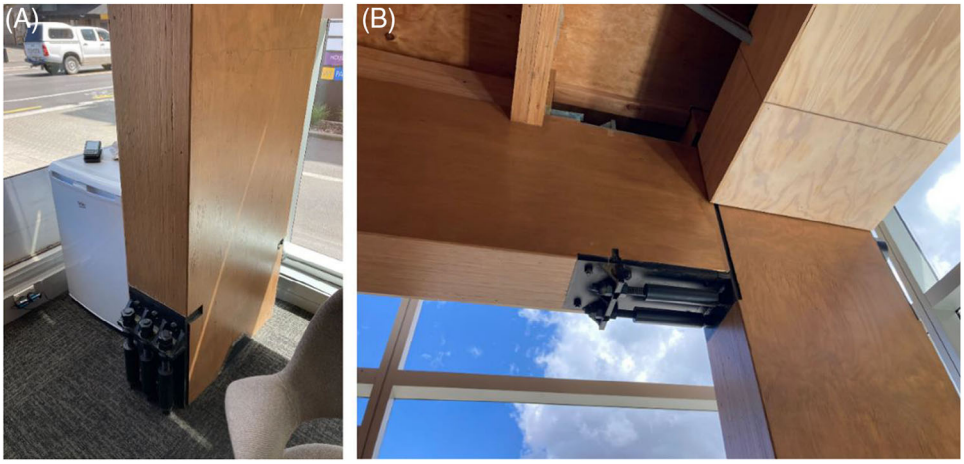

FIGURE 2 Example of (A) column-to-foundation connection and (B) beam-column connection with external damping devices, Young Hunter House, 'Merritt Building', Christchurch (NZ) (pictures courtesy of G. Formichetti).

advantages of this system are not only limited to its outstanding performance: the wooden elements are relatively easy to prefabricate, transport, and assemble, making it a prime solution for a lot of different buildings' applications (e.g.,[37–41]) (e.g., Figure 2). Meanwhile, some solutions combining different materials were also investigated, such as a combination of reinforced concrete columns with timber beams (e.g.,[29,42–44]) to reduce the issue of loading perpendicular to grain in beam-column joints.

As part of a continuous development, in order to properly evaluate the performance of these systems, there is a need for a comprehensive framework for the definition of fragility curves to describe the system vulnerability at building and component levels. While the building's fragility curves enable the evaluation of the safety and reliability of the global structural system, the components' fragility models allow for a more thorough analysis of the damage and related economic losses due to the seismic action. Despite the large amount of research and investigations in the literature conducted on structural systems incorporating walls (e.g.,[45–49]), a comprehensive framework for the estimation of fragility curves for moment-resisting Pres-Lam frames has not yet been fully developed. Worth acknowledging the work by Granello et al.[50] that proposed a methodology for estimating the time-dependent fragility functions of structural components considering the impact of post-tensioning losses due to the visco-elastic nature of timber. The Multiple Stripes Analysis method (MSA)[51,52] is used by the authors to characterize the global performance of the building regarding the Serviceability Limit State (SLS), Ultimate Limit State (ULS), and Collapse prevention Limit State (CLS).

Assessing the structural fragility is a fundamental step within the Performance-Based Earthquake engineering framework (PBEE).[53] The use of a probabilistic-based framework is necessary to account for aleatoric uncertainties of the seismic action, to the so-called record-to-record variability, and epistemic uncertainties associated with component capacity, material proprieties and construction details. Within this context, several methodologies have been developed so far to assess the seismic vulnerability and risk—in the form of fragility curves—of buildings thought static and dynamic analyses. The most used method is the incremental dynamic analysis (IDA),[54] which relies on a suite of progressively scaled ground motions to find the intensity measure that brings the structure on the onset of a defined Limit State (LS) using nonlinear time-history analyses (NLTHAs). However, this methodology requires multiple dynamic analyses to be performed to obtain a single data point making it computationally demanding. Reducing the number of iterations is key to speeding up the procedure. Therefore, many authors proposed more efficient algorithms and methodologies to reduce the number of steps and take advantage of modern computer architecture.[52,55] Furthermore, other methodologies have been proposed to reduce the computational demand such as the MSA[56,57] or the Cloud Method.[56,58,59] The latter requires less computational effort but more attention to the ground motion selection. Although the Cloud procedure relies on several assumptions (i.e., the constant conditional standard deviation for the probability distribution of the engineering demand parameter given the intensity measure, and the dependence on the suite of input motions), it allows accounting for the record-to-record variability using unscaled ground motions as well as including epistemic uncertainties. Modeling and material uncertainties can be considered by combining the Cloud Methodology and sampling approaches.[60] Moreover, the methodology was further developed to account for collapse cases.[61]

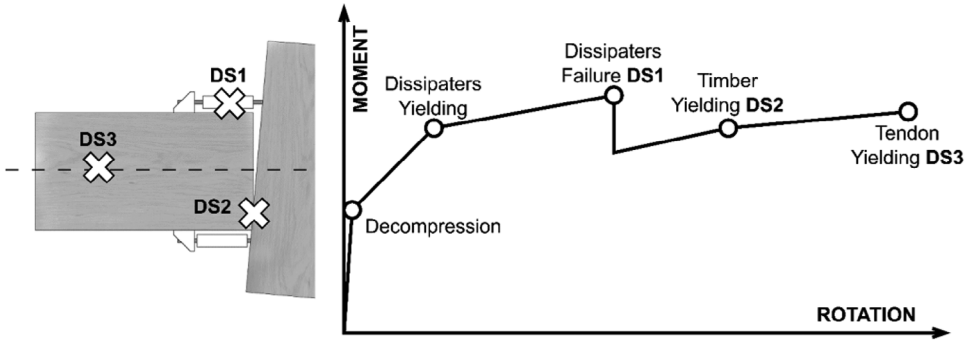

FIGURE 3 Overview of the beam-column connection Damage States within a conceptual moment-rotation curve.

This article proposes a framework for the estimation of fragility models for single structural components of Pres-Lam frames considering the principal local damage states of the sections and accounting for the record-to-record variability. The analysis was conducted by implementing IDA, due to its widespread use, and the Cloud methodology, due to its lower computational demand than the IDA procedure. Finally, the data obtained through the Cloud methodology were processed to fit fragility models at a component level. To this end, a parametric model of Pres-Lam frames was developed to conduct analyses on multiple case studies using the OpenSEES Framework through the Python Application Programming Interface (API).[62,63] Three different limit states were investigated related to damage to the structural components.

2 | METHODOLOGY

This article is composed of two parts: the first one investigates the computation of building-level fragility curves, to be used in loss and risk assessment methodologies, and the second one tackles the definition of fragility function for structural elements, to be used in component-based loss-assessment methodologies. All the fragility curves are investigated and computed relative to three damage states involving the hybrid rocking connections: (i) failure of the external damping devices, (ii) yielding of the timber at the interface of the connections, and (iii) yielding of the post-tensioning cables.

To achieve the first goal, fragility functions were developed by employing two different wide-spread methodologies: (i) the IDA[54] and (ii) the Cloud method, proposed by Jalayer et al.[60] and revised by Jalayer et al.[61] to include collapse cases. Furthermore, the Cloud methodology has been applied following two different approaches: in the first approach, the onset of limit states is monitored by means of a demand capacity ratio (DCR), evaluated by investigating the local mechanisms of the structural elements, while in the second approach, the onset of damage states is monitored by means of maximum inter-storey drifts. The threshold values of inter-storey drift associated with the onset of the limit states are defined by performing a nonlinear static pushover (PO).

Finally, to obtain fragility curves for the structural component, the Cloud methodology has been employed.

2.1 | Limit states

Due to the different mechanism and behaviour of low-damage structures under seismic loading, when compared with traditional reinforced concrete (RC) or other traditional timber structures, specific Damage (Limit) States should be defined and adopted for the structural elements and connections of this innovative technology.

In this article, three Limit States (or Damage States DS) are considered for the low-damage structural components (Figure 3): (i) DS1, defined as the failure of external dissipaters (slight damage), (ii) DS2, defined as the yielding in compression of the timber (moderate damage), and (iii) DS3, defined as the yielding of unbonded tendons (extensive damage). The definition is consistent with the ones proposed by Bianchi et al.[65] for PRESSS low-damage connections with respect to the slight and the extensive damage state, with the addition of an intermediate damage level. In fact, the moderate damage state accounts for the susceptibility of timber components, which replace RC elements from the PRESSS technology, to yielding along the grain. This means that beams and columns may experience plastic deformations in the timber when they reach the compression strength at the connection interface. The severity of this damage state

TABLE 1 Comparison between damage levels for monolithic traditional and low-damage solution.

Damage level	RC monolithic frame	PRESSS	Pres-Lam
Slight	Residual cracks > 0.06 inches (1.5 mm)	Failure of external damping devices	Failure of external damping devices
Moderate	Initial spalling of concrete	–	Timber yielding parallel to grain
Extensive	Concrete core crushing	Yielding of post-tensioned element	Yielding of post-tensioned element

is lesser than the yielding of the tendon elements, which failure jeopardizes the structural integrity of the connection, but is greater than the failure of external damping devices. This is to say, the yielding of the timber interface, despite not directly compromising the structural connection, it is more difficult to repair than the failure of the external damping devices, which are easily swappable by design (Table 1).

It is worth noting that, even if the definition of the damage states is analogue to the ones defined for the traditional monolithic RC frame elements, they are conceptually different. In fact, damage state for classic RC elements are usually considered as (i) residual crack widths > 0.06 inches or 1.5 mm (slight damage), (ii) initial spalling of cover concrete (moderate damage), and (iii) concrete core crushing (extensive damage), according to FEMA P-58.[64] It should be noted that the rupture of external damping devices not only is less expensive to repair in term of both downtime and dollars when compared to the residual cracks in the concrete element, but also is expected to occur for higher intensity earthquakes. In fact, while the slight damage in low-damage components (i.e., failure of external damping devices) is expected/designed to occur after ultimate limit state earthquake intensity,[66] the slight damage in traditional concrete elements (i.e., residual cracks wider than 1.5 mm) is expected/designed to occur after serviceability limit state earthquake intensity. On the other end, moderate damages become much more comparable between the two technologies despite the yielding of the timber is expected to occur for higher earthquake intensities than the concrete spalling, as the cost related to such repairs might be considered alike. Finally, the yielding of the post-tensioning element can be considered similarly to concrete crushing as the extensive damage level.

It is worth noting that two limit states—the rupture of the tendons and the splitting of the timber—are not explicitly considered in this study. These damage mechanisms are expected to occur only after the tendons have yielded (DS3). However, beyond DS3, the behaviour of the section becomes increasingly uncertain, and as a result, these damage mechanisms were not investigated. To proceed with this assumption, it is essential to verify during the design phase that the desired sequence of damage states is achieved.

2.2 | Overview of the selected methodologies

Fragility curves are used to define the probability of exceedance of a damage state as a function of either an intensity measure (IM), for building-level curves, or an engineering demand parameter (EDP), for component-level functions.

The chosen methodologies to develop fragility functions are, as stated previously, the IDA and the Cloud method.

The IDA was applied to investigate the IM leading to a global DCR of 1 for all the considered limit states. The procedure is described in detail by Vamvatsikos and Cornell,[54] while main formulations are reported below.

Once the data points composed of IMs leading to the onset of the Limit State (LS) are obtained, the fragility model is fitted using a lognormal distribution:

$$P\ [DCR_{LS} > 1 | IM\ =\ im] =\ CDF\left(\frac{ln\,(im/\theta_{IM})}{\beta_{DCR_{LS,IDA}}}\right) \tag{1}$$

$$ln\,\theta_{IM} = \frac{1}{n}\ \sum_{i}^{n} lnIM_i \tag{2}$$

$$\beta_{DCR_{LS,IDA}} = \sqrt{\sum_{i}^{n} (ln\,(IM_i/\theta_{IM}))^2/\,(N-1)} \tag{3}$$

where CDF stands for cumulative distribution function of the normal standard distribution, $ln\theta_{IM}$ is the natural log of the average IM leading to the LS, and $\beta_{DCR_{LS,IDA}}$ is the lognormal standard deviation related to the LS.

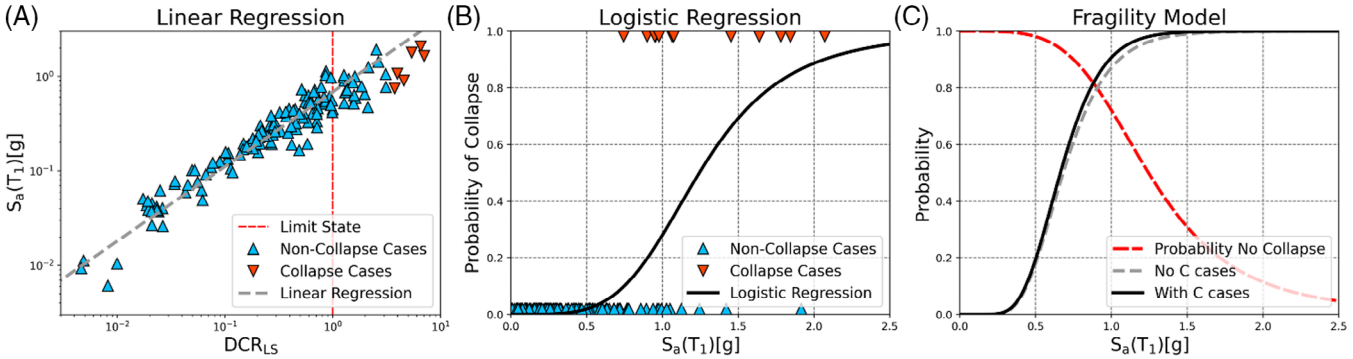

FIGURE 4 Fragility model procedure accounting for collapse cases.

Differently from the IDA, the Cloud methodology uses a suite of unscaled ground motions to characterize the structural response through NLTHAs. The probability of exceedance can be computed for each LS as a sum of the probability of exceedance of the investigated LS given the structure did not incur in a collapse, and the probability of the structure collapsing under the seismic action Jalayer et al.[61]:

$$P\ [DCR_{LS} > 1|IM] = P\,[DCR_{LS} > 1|IM, NoC] \cdot (1 - P\,[C|IM]) + P\,[C|IM] \tag{4}$$

where $P[DCR_{LS} > 1|IM, NoC]$ is the probability of exceedance of the limit state given the structure did not collapse and $P[C|IM]$ is the probability of collapse given the IM.

The probability of exceedance can be described once again using the cumulative density function of a lognormal distribution:

$$P\ [DCR_{LS} > 1|IM, NoC] = CDF\left(\frac{E\,[lnDCR_{LS}|IM]}{\beta_{DCR_{LS}}}\right) \tag{5}$$

where $E[lnDCR_{LS}|IM]$ is the expected value of the natural logarithm of the DCR given an IM and $\beta_{DCR_{LS}}$ is the associated standard deviation.

The expected value of $lnDCR$ can be computed for the selected LS by fitting a linear regression in log-log space (Figure 4A):

$$E\ [lnDCR_{LS}|IM, NoC] = lna + b \cdot lnIM \tag{6}$$

where lna and b are the fitting parameters for the linear regression. The data points are here limited to No Collapse (NoC) cases because, even if sometimes a DCR can be computed for the collapse cases, they tend to deviate from the linear regression and their inclusion in the dataset will result in a reduction of the regression's slope and an increase of dispersion.

To assess the dispersion, the logarithmic standard deviation $\beta_{DCR_{LS}}$ is computed:

$$\beta_{DCR_{LS}} = \sigma_{lnDCR_{LS}} = \sqrt{\sum_{i}^{n} \left(lnDCR_{LS,i} - E\,[lnDCR_{LS}|IM_i, NoC]\right)^2 / (N-2)} \tag{7}$$

where $E[lnDCR_{LS}|S_{a,i}(T_1), NoC]$ is given by Equation 6 and N is the number of data points.

The collapse probability can be modelled using a logistic regression model as a function of the natural log of IM (Figure 4B):

$$P\ [C|IM] = \frac{1}{1 + e^{-(\alpha_0 + \alpha_1 \cdot lnIM)}} \tag{8}$$

where α_0 and α_1 are the logit regression parameters. The use of the natural log of the intensity measure ensures that the probability of collapse approaches 0 as the IM goes to 0.

2.3 | Development of building-level fragility curves

The first mode on spectral acceleration, denoted as $S_a(T_1)$, was chosen as the intensity measure (IM) to compute the building-level fragility curves, as typically considered for reinforced concrete (RC) structures. The performance was evaluated using the *DCR* for all the desired Limit States (*LS*), denoted as DCR_{LS}. $DCR_{LS,j}$ were initially computed for all the structural components of the building for each chosen limit state, and then combined to obtain a global value of DCR_{LS}:

$$DCR_{LS} = max_j^{Ncomp} DCR_{LS,j} = max_j^{Ncomp} \frac{D_j}{C_j\,(LS)} \tag{9}$$

where $Ncomp$ is the number of structural components of the structure, D_j is the demand for the j-component, and $C_j(LS)$ is the capacity of the j-component relative to a given limit state.

Therefore, in the first approach, performed for both Cloud Methodology and IDA, the gap opening of the section was recorded at each integration step of the time history analysis to find the maximum absolute gap opening for each low-damage structural component. Then, the maximum value of the gap opening was divided by the gap opening associated with the onset of the *LS* as computed in the moment-rotation calculation phase. Finally, the highest ratio between demand and capacity among all the components was identified as the global *DCR*. In particular, the IDA was performed until either the *DCR* of 1 was exceeded or the dynamic instability of the model was reached.

In the second approach, static non-linear pushover analyses were performed to investigate the relationship between *DCR* and inter-storey drift ratios. Following this approach, the gap openings in the low-damage connections were monitored during the pushover analysis to find the maximum inter-storey drift ratio associated with a value of the *DCR* equal to 1. Finally, the Cloud methodology was performed using the maximum inter-storey drift ratio as the new EDP, greatly simplifying the post-processing effort.

2.4 | Development of component-level fragility curves

Fragility models for the structural components were fitted using the resulting data from the NLTHAs. The chosen engineering demand parameter (EDP) was the inter-storey drift ratio, for consistency with the FEMA P-58[64] methodology. The EDP was then used to define the structural subassemblies' failure probability. The model was fitted using the Cloud methodology without considering collapse cases. For each case study, the *DCR* of the connection was computed using the maximum gap-opening recorded during a NLTHA, as described above, and the EDP was chosen to be the maximum inter-storey drift that occurred at the connection's corresponding floor. The data points were collected for all the different types of connections in the model for the multiple case-study buildings.

Finally, failed analyses resulting from dynamic instability were excluded from the dataset, as well as analyses that reached an inter-storey drift of more than 10%. Additionally, analyses that did not exhibit an inter-storey drift above 0.05% were also excluded from the dataset because the ground motions were not strong enough to engage the structural connections.

2.5 | Development of a parametric framework

A parametric workflow was developed to analyse a variety of case-study buildings (Figure 5). The workflow begins by leveraging the building data (structural and non-structural components) stored in a building information model (BIM) developed in Revit. To isolate and export the structural properties needed for the seismic structural analysis, a Dynamo script was developed. This script collects section details, structural framing, and floor masses, and combines them into a JavaScript Object Notation (JSON) format.

This JSON file is then fed into a Python pipeline through the OpenSEES application programming interface (API). The pipeline starts by performing moment-rotation analysis of the structural elements and identifying gap openings associated with the onset of focused limit states. These data are used to define link (spring) properties modelling the behaviour of the hybrid connections. Thus, the Python pipeline builds the model according to the instructions in the JSON file, incorporating the data obtained in the previous step. Once the model is created, simulations are run according to a secondary

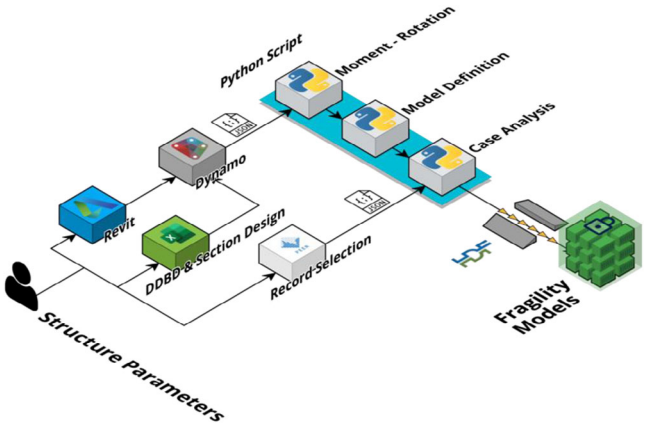

FIGURE 5 Overview of the parametric workflow.

JSON file. Both pushover nonlinear analyses and time history nonlinear analyses can be performed as specified in this file. Details over the moment-rotation and the numerical modelling can be found in Chapter 5.

To optimize processing power and efficiency, the workflow implements a parallel processing approach by creating multiple concurrent processes, particularly for running several time history analyses required by the Cloud and IDA methodologies. The code for this workflow is available on GitHub: https://github.com/ChimieleCode/preslam-ops-engine.

After completing the analyses, the output data are collected and organized into a Hierarchical Data Format (HDF) file format. HDF can be very helpful for handling large and diverse datasets due to its ability to efficiently store and retrieve data. Once the data is organized, a series of post-processing scripts are run to extract valuable insights about the building's performance. For example, fragility models can be fitted to the data to predict the building's vulnerability to future earthquakes. The post-processing scripts may also be used to generate visualizations or data reporting for further analysis.

3 | CASE STUDIES

The fragility estimation procedure was carried out on three multi-storey timber buildings. The case-study buildings were chosen to be representative of a wide range of possible implementations of the Pres-Lam technology spanning from three to eight floors with different sections, reinforcement detailing, and floor plans. The horizontal earthquake-resistant systems consist of frames along the longitudinal direction and walls along the transverse direction. For the scope of this article, the focus will be solely on evaluating the performance of the frames. Structural schemes of all case studies are reported in Figure 6, while overall structural properties are summarized in Table 2.

The building use is commercial, and the structural systems are designed for gravity loads and seismic loads. The latter are defined considering the seismicity of a high earthquake-prone area situated in the centre of the Italian peninsula (L'Aquila, C soil type as defined by NTC2018[67]), which suffered a devastating earthquake in 2009.

For all the case studies, the frames' structural members are made of laminated Veneer Lumber (LVL) (LVL44 type, bending stress 44 MPa, Young's modulus 13.8 GPa). Mild steel external damping devices are built by means of S355 steel grade according to NTC2018.[67] Finally, as tendons, multiple T15.7 super 7-wire strands are considered from existing catalogues (i.e., ArMi T15.7 super from ArcelorMittal, yielding stress 1670 MPa). A detailed overview of the assumed material proprieties is available in Table 3. The considered floor system is the Timber Concrete Composite (TCC[68,69]).

4 | SEISMIC DESIGN

The design procedure for the case-study buildings was carried out using the direct displacement-based design (DDBD) approach proposed by Priestley et al.[70,71] and then extended to low-damage systems by Pampanin.[72] A two-step procedure proposed in Miliziano et al.[73] was implemented as shown in Figure 7. Due to the lower stiffness of timber elements

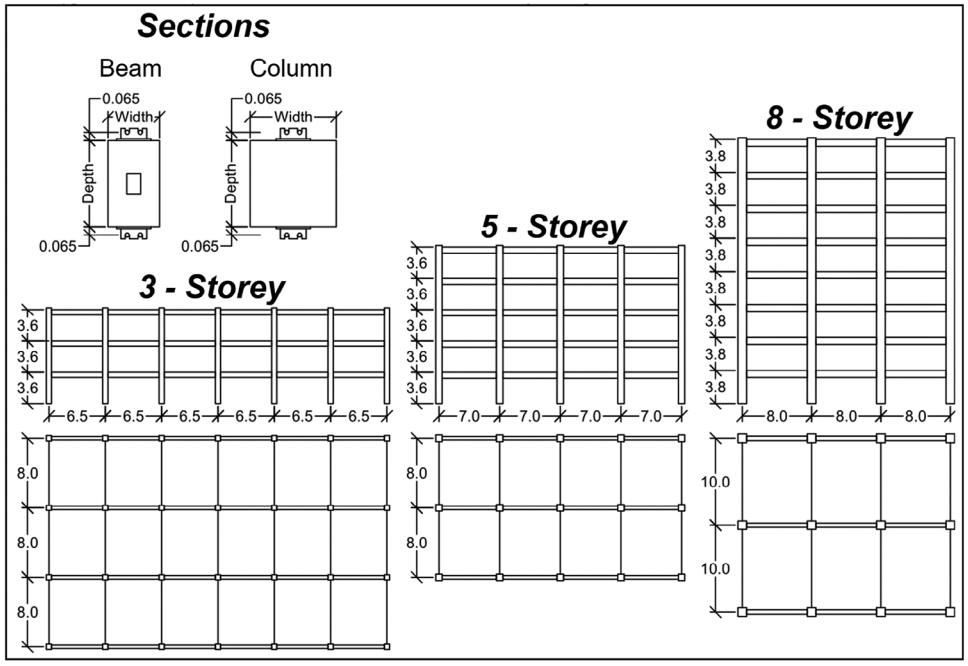

FIGURE 6 Plan view of the floors, lateral view of the frames, and sketch of components' sections (note: units are in meters).

TABLE 2 Properties of the case-study buildings.

Case	3-storey	5-storey	8-storey
Stories	3	5	8
Spans	6	4	3
Frames	4	3	3
Span length	6.5 m	7 m	8 m
Inter-storey height	3.6 m	3.6 m	3.8 m
Floor mass	763 ton	389 ton	444 ton
Roof mass	527 ton	270 ton	314 ton
Column depth	0.7 m	0.75 m	1.0 m
Column width	0.6 m	0.75 m	1.0 cm
Beam depth	0.7 m	0.7 m	0.8 m
Beam width	0.4 m	0.4 m	0.5 m

TABLE 3 Material proprieties.

Timber grade	f_b (MPa)	$f_{c,0}$ (MPa)	E_0 (GPa)	E_{90} (GPa)	G (GPa)
LVL44	44	35	13.8	0.43	0.60
Steel grade	**f_b (MPa)**	**f_u (MPa)**	**E_s (GPa)**	**ε_y (%)**	**r (-)**
S355	355	510	210	0.17%	0.079
Tendon name	**Ø (mm)**	**A (mm^2)**	**$f_{pt,k}$ (MPa)**	**$f_{pt01,k}$ (MPa)**	**E_p (GPa)**
ArMi 6″ super	15.7	150	1860	1670	201

compared to concrete ones, the Serviceability Limit State (SLS) typically governs the sizing of structural components and post-tensioning force. However, the design of the sections must be checked against Ultimate Limit State (ULS) to ensure structural members have sufficient redundancy and ductility.

The buildings were designed to not exceed 0.5% of inter-storey drift, θ_{design}, as required by the Italian Building Code NTC2018[67] at the SLS (referred to as SLD, damage limit state, in the Italian Building Code). The low-damage connections were designed to achieve a global recentring ratio (β) of 0.6 (ratio between the recentring capacity, provided by tendons

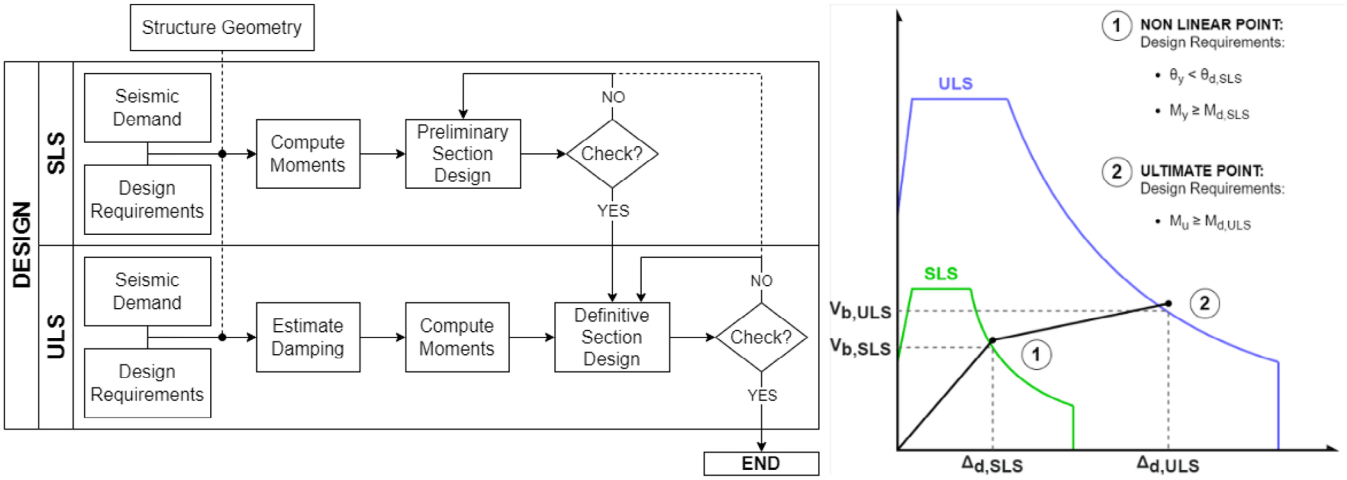

FIGURE 7 Design procedure accounting for SLS and ULS performance (Modified after Miliziano et al.[73]).

TABLE 4 Design parameters.

Parameter	3-storey		5-storey		8-storey	
	SLS	ULS	SLS	ULS	SLS	ULS
Design drift level, θ_{design} (%)	0.5	1.7	0.5	1.8	0.5	1.75
Design displacement, Δ_{design} (m)	0.040	0.135	0.063	0.188	0.104	0.298
Effective mass, $m_{effective}$ (ton)	1750	1750	1490	1565	2714	2848
Effective height, $H_{effective}$ (m)	7.96	7.96	12.65	12.32	20.92	20.38
Equivalent damping ratio, ξ_{eq} (%)	5	8.4	5	7.2	5	6.7
Effective period, $T_{effective}$ (s)	0.81	1.39	1.28	1.82	2.12	2.81
Effective stiffness, $K_{effective}$ (kN/m)	106540	35801	43853	18748	23933	14275
Base shear, V_{base} (kN)	4241.2	4845.7	2272.6	3529.4	2503.1	4255.7

TABLE 5 Connection details.

Component	3-storey		5-storey		8-storey	
	Mild steel	Tendons	Mild steel	Tendons	Mild steel	Tendons
Beam—Floor 8	–	–	–	–	2 Ø 16 mm	4 @ 550 kN
Beam—Floor 7	–	–	–	–	2 Ø 16 mm	5 @ 700 kN
Beam—Floor 6	–	–	–	–	3 Ø 16 mm	6 @ 850 kN
Beam—Floor 5	–	–	2 Ø 14 mm	3 @ 400 kN	3 Ø 16 mm	7 @ 1000 kN
Beam—Floor 4	–	–	2 Ø 14 mm	4 @ 650 kN	3 Ø 16 mm	7 @ 1100 kN
Beam—Floor 3	2 Ø 16 mm	4 @ 450 kN	3 Ø 14 mm	6 @ 900 kN	3 Ø 18 mm	8 @ 1300 kN
Beam—Floor 2	2 Ø 16 mm	5 @ 750 kN	3 Ø 14 mm	7 @ 1050 kN	3 Ø 18 mm	9 @ 1400 kN
Beam—Floor 1	2 Ø 16 mm	6 @ 900 kN	3 Ø 14 mm	7 @ 1100 kN	3 Ø 18 mm	9 @ 1500 kN
Column	2 Ø 20 mm	–	2 Ø 20 mm	–	3 Ø 20 mm	–

and axial load, and the mild steel capacity, given by external Plug and Play damping devices) at the ULS, targeting a drift around 1.7%–1.8%. All the DDBD parameters for SLS and ULS limit states are reported in Table 4, while the connection details are provided in Table 5.

The beam-column joint details were designed using a 10 mm steel plate on each side of the column interface. These steel plates are connected to each other by steel rods passing through the column. These connection details play a crucial role in enhancing the stiffness of the joint, which is loaded perpendicular to the grain, but also in limiting the post-tensioning losses in the tendons, as shown by Granello et al.[74] A schema of the beam-column connections is presented in Figure 8. To account for the reduced stiffness at the connections' interface, the timber Young modulus, Econ, in the

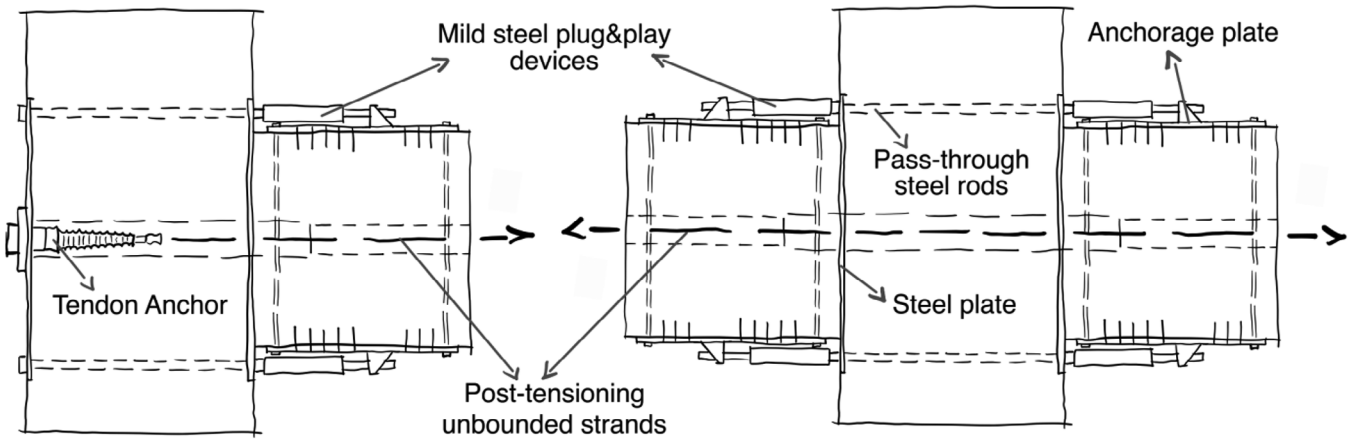

FIGURE 8 A sketch of the connection details for both external and internal beam-column joints.

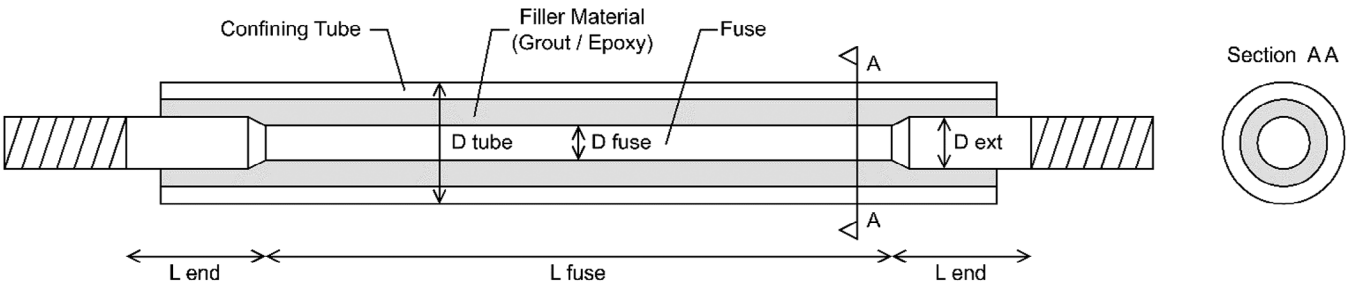

FIGURE 9 Schematic of the external replaceable 'Plug&Play' damping device (modified after Sarti et al.[22]).

beam-to-column connection was reduced by 30% (equivalent to a connection stiffness coefficient of 0.7) and by 45% in the column-to-foundation interface (equivalent to a connection stiffness coefficient of 0.55) as described in Design Guidelines for Post-Tensioned Timber Buildings[66] and Miliziano et al.[43]

The tendons are positioned along the centre line of the beams, and the external damping devices are placed 6.5 cm above and below the timber section in both beams and columns. All the connections are equipped with shear keys to avoid relying entirely on the shear friction mechanism. External damping (Figure 9) devices are designed to have a slenderness ratio between 40 and 60 for optimal performance.

The Plug& Play steel dissipators were designed to undergo an axial deformation in the range of 2%−4% at ULS. This enables sufficient plastic reserves while maximizing the effectiveness of the devices. The tendon demand deformation computed at ULS was limited to 70% of capacity-yielding deformation. Finally, the timber deformation in compression was checked to avoid overcoming 0.25% in beam-column joints and 0.35% in column-foundation connections, thus considering the reduced stiffness of the timber interface.

5 | NUMERICAL MODELLING

To simulate the response of low-damage timber buildings, several analytical and numerical models have been developed by different authors (e.g.,[50,73,75–77]). These models employ lumped-plasticity approaches and explicitly consider the contributions of unbonded tendons, mild steel, and joint stiffness in beam-column connections, while a multi-spring model or rotational springs for describing the column-to-foundation contact. Moreover, the concept of 'monolithic beam analogy' has been used to assess the moment-rotation relationship of hybrid low-damage connections. This procedure, originally introduced by Pampanin et al.,[78] relies on an iterative approach and takes into account *member compatibility* (since local compatibility is no longer satisfied in a rocking connection due to the gap opening). The procedure has been further developed by Palermo,[79] adapted to Pres-Lam by Newcombe et al.,[31] and later revised by Smith.[80]

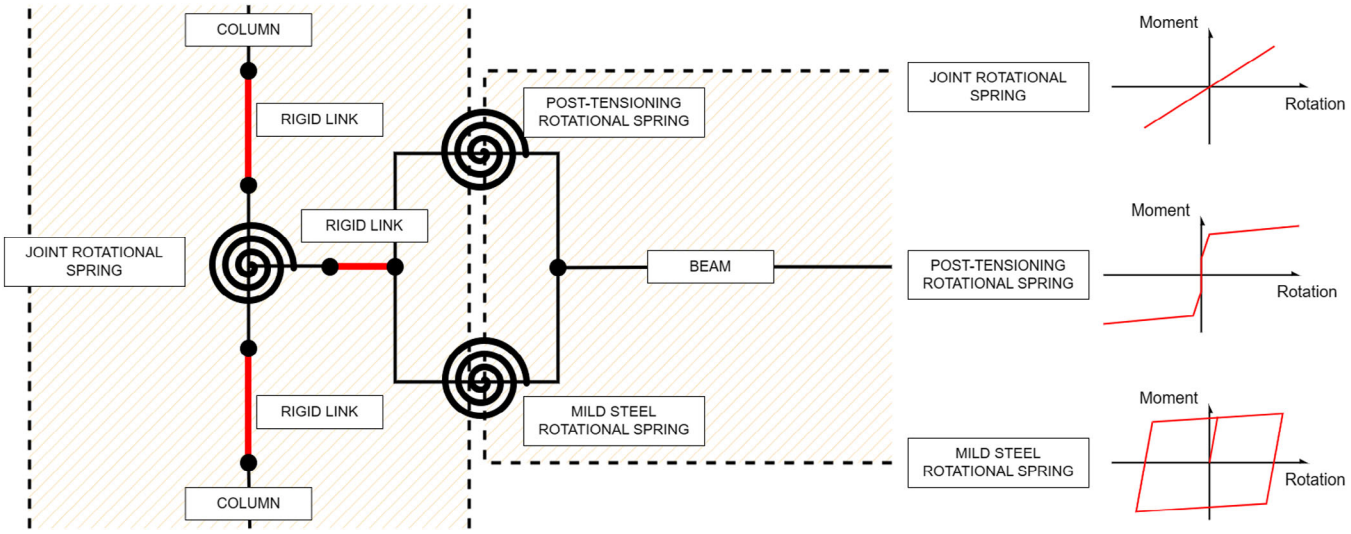

FIGURE 10 Modelling of hybrid low-damage connection for a beam-column joint.

Considering the available modelling techniques, a lumped plasticity approach was selected for this work, due to its demonstrated accuracy in predicting the behaviour of connections in Pres-Lam frames.[81]

Specifically, the beam-column connection was modelled accounting for three different contributions (Figure 10):

- the post-tensioning unbonded tendons were modelled as a multi-linear elastic link;
- the mild steel was modelled through the Giuffrè-Menegotto-Pinto (GMP, Steel02) hysteretic behaviour;
- the joint shear deformation was modelled using an elastic link.

The mild steel contribution was set to fall to zero once the axial deformation inside the external bars reaches 6%. Moreover, the connection was considered to fail once the yielding deformation of the unbonded tendons is exceeded, as the re-centring and gap-closing capabilities of the elements are compromised. The multi-linear elastic and Steel02 links were wrapped into a MinMax material, available in the OpenSEES library, to model the failure of the steel and post-tensioning contributions. When the timber reaches its yielding point under compression, the moment-rotation relationships was computed by considering a partially plasticized interface, thus reducing the stiffness of the connection following a simplified elastoplastic behaviour.

The joint elastic link stiffness (K_{joint}) was obtained based on the formulation proposed by the Design Guide for Post-Tensioned Timber Buildings[66]:

$$K_{joint,int} = \frac{4}{3} \frac{\alpha_{s,ave} A_{col} h_b G_t}{\left(1 - \frac{h_c}{L}\right)(2 - \beta)} \tag{10}$$

$$K_{joint,ext} = \frac{2}{3} \frac{\alpha_{s,ave} A_{col} h_b G_t}{\left(1 - \frac{h_c}{L}\right)} \tag{11}$$

where:

- $\alpha_{s,ave}$ is the effective shear area assumed as 0.85 for rectangular beams;
- A_{col} is the area of the column;
- h_b is the height of the beam;
- G_t is the shear modulus of the timber;
- β is the ratio of the effective height of the beam assumed as 2/3.

The column-foundation connections were modelled using only the multilinear-elastic link and the GMP link to account for the contributions of axial load and external dampers, respectively.

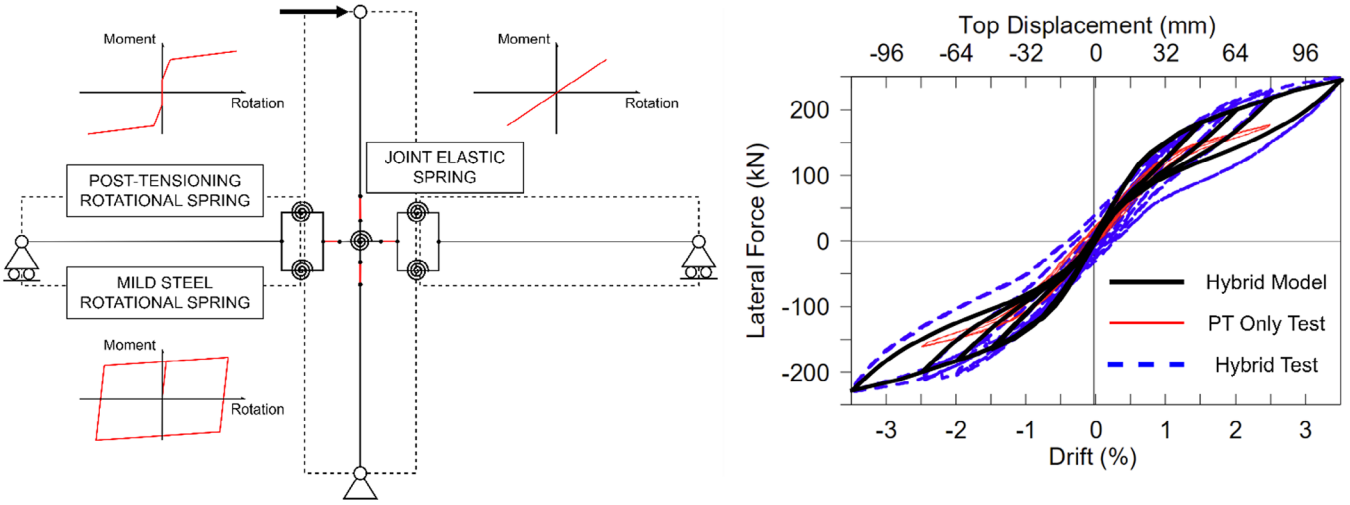

FIGURE 11 Details of the numerical modelling of the specimen tested by Iqbal et al.[32] (A) and numerical vs. experimental comparison (B).

TABLE 6 Comparison between numerical and experimental parameters.

Parameter	Numerical	Experimental	Difference
Peak averaged lateral force (kN)	237.7	239.0	+ 0.55%
Effective stiffness at peak force (kN/m)	2122	2164	+ 1.98%
Effective damping last cycle (%)	8.66	9.55	+ 10.3%

Finally, the vertical loads were applied to the joint nodes, as well as the seismic masses. The diaphragms, due to the presence of concrete slab in the TCC floors, were modelled as rigid using an *equalDof* (OpenSEES) constraint along the horizontal translational direction for each floor.

6 | NUMERICAL VALIDATION

In addition to the extensive numerical versus experimental validation carried out in literature (e.g.,[31,50,73,75–77,81]), the modelling approach described in the previous chapter (Chapter 5) was directly validated against numerical testing to assess the accuracy of the developed workflow.

More specifically, a numerical model was implemented within OpenSEES to simulate a structural system described in the experimental testing performed by Iqbal et al.[32] The specimen is an internal beam-to-column joint with external mild-steel dissipaters. The specimen is equipped with 12–12.7 mm tendons, which are subjected to a total stress of 965 kN, and 8–16 mm external damping devices. A 30% reduction was considered in the parallel-to-grain stiffness when addressing the moment-rotation relationship, based on the assumption described above. The details of the model and of the numerical versus experimental validation can be found in Figure 11.

The numerical result shows a good agreement with the experimental result up to a drift of 2.5%, despite underestimating residual displacements. The simplified assumption about the plastic behaviour of the timber was able to accurately predict the reduction in stiffness of the backbone curve. However, it was unable to capture the effects of timber yielding on the hysteretic behaviour of the connection, including the increase of residual displacements. This is since the reduction in stiffness caused by timber yielding along the grain interface is mainly taken into account by the multi-linear elastic link modelling the tendons recentring behaviour. This leads to a non-negligible underestimation of the hysteretic energy of the connection for larger cycles, as shown in Figure 11. Nonetheless, this approach is conservative. A comparison between the experimental data and the numerical results is presented in Table 6, which demonstrate the effectiveness of the proposed model.

TABLE 7 Threshold interstorey drift ratios for each damage state computed from the pushover analysis, and the first mode period computed from the modal analysis.

Analysis	Parameter	3-storey	5-storey	8-storey
Pushover	DS1 Interstorey Drift Ratio (%)	2.61	2.14	1.96
	DS2 Interstorey Drift Ratio (%)	4.08	3.03	2.50
	DS3 Interstorey Drift Ratio (%)	6.24	4.97	5.11
Modal	First mode period (s)	0.795	1.038	1.589

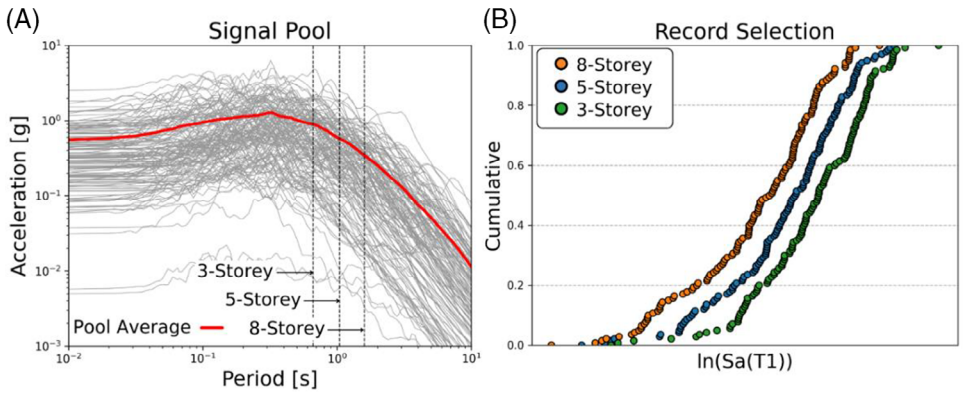

FIGURE 12 Response spectra for each record in the selected pool (A) and the distribution of intensity measures for each case study (B) for the Cloud analysis.

7 | FRAGILITY STUDY: RESULTS AND DISCUSSION

In this section, the fragility study and related results are presented along with the pool of records used to carry out the analyses.

7.1 | Record selection

Fragility curves were developed using IDA and Cloud methodologies using two different pools of ground motions.

To perform the IDA, a total of 44 ground motions (22 for each direction) provided by the FEMA P-695[82] guidelines for assessing the seismic performance of buildings were used.

The ground motions used for the Cloud methodology were selected according to the case study, making the record-selection process more time consuming. The main considerations for ground motion selection, as recommended by Jalayer et al.,[60] should be:

- The records need to cover a wide range of the chosen intensity measure in order to make a good linear fit in logarithmic scale;
- A good portion of the records—ideally 30%—should reach the desired damage level;
- Avoid selecting too many ground motions from the same earthquake event.

One hundred and forty-one different ground motions were selected from the NGA PEER West2 Database[83] as described in Jalayer et al.[84] The selected ground motions' spectra, as well as the intensity measures for all the three different case studies, are shown in Figure 12.

Due to the high seismic performance of low-damage structural systems, the desired ratio of 30% of exceedance for DS2 and DS3 could not be achieved using unscaled ground motions. Despite that, decision was made to continue with the current suite of records without recurring to a scaling procedure.

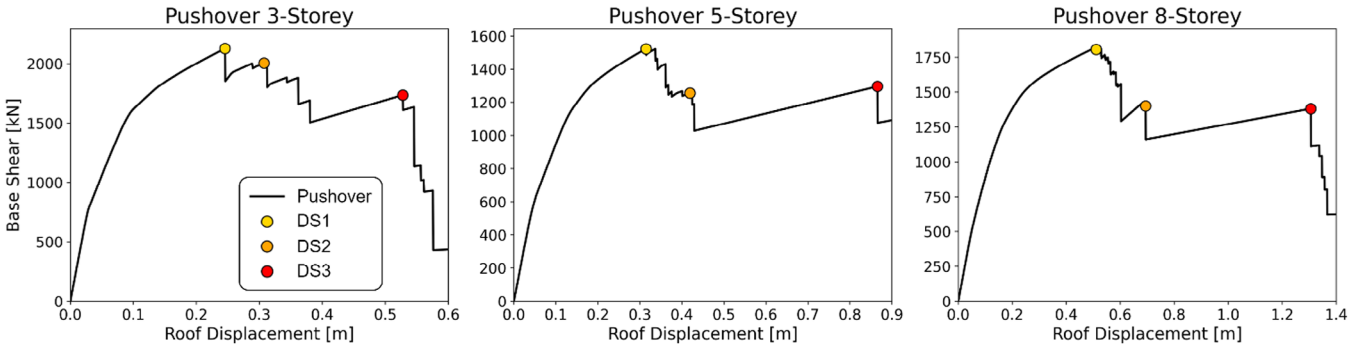

FIGURE 13 Pushover curves for the case-study frames.

TABLE 8 Median (μ) and Standard Deviation Beta (β) values for all the fragility curves.

Case	Damage state	IDA		Cloud NoC+C		Cloud NoC		Cloud PO	
		μ	β	μ	β	μ	β	μ	β
3-storey	DS1	0.967	0.360	0.975	0.253	1.023	0.334	1.048	0.250
	DS2	1.155	0.397	1.364	0.299	1.607	0.346	1.455	0.333
	DS3	1.396	0.439	1.614	0.380	2.287	0.352	1.655	0.457
5-storey	DS1	0.600	0.246	0.664	0.320	0.682	0.429	0.713	0.287
	DS2	0.777	0.276	0.937	0.274	1.047	0.379	0.962	0.269
	DS3	0.987	0.378	1.183	0.334	1.904	0.460	1.215	0.300
8-storey	DS1	0.360	0.450	0.385	0.384	0.390	0.471	0.446	0.319
	DS2	0.478	0.410	0.591	0.297	0.637	0.399	0.565	0.301
	DS3	0.641	0.402	0.786	0.304	1.134	0.444	0.829	0.314

7.2 | Structure-level fragility curves

The analyses were carried out by means of the workflow defined in the methodology section. The pushover analyses were first performed for each case-study to verify that the desired hierarchy of mechanisms (steel failure, timber yielding, and tendon yielding) was always respected, as shown in Figure 13.

The maximum inter-storey drift relative to the onset of the limit state was recorded for each case study. This recorded value was used as the capacity parameter to compute the DCR in the Cloud methodology based on the inter-storey drift monitoring approach. Results obtained from all the above-mentioned procedures are compared in Figure 14. Fragility curves parameters are reported in Table 8.

In addition to the pushover, a modal analysis was performed for each case study structure to compute the first response period. Results are reported in Table 7.

The results indicate that for the DS1 limit state, all the proposed procedures yield comparable outcomes. Notably, the Cloud methodology achieves an exceedance ratio of unscaled ground motions that is close to the desired 30% for this limit state. However, for the DS2 and DS3 limit states, the Cloud methodology consistently overestimates the median of the curve in comparison to the IDA methodology. It should be noted that the two procedures were conducted using different sets of records. Nevertheless, this discrepancy may be attributed to the high scale factors required to bring the structure to the onset of such limit states, which in some instances approached a value of 10.

Moreover, results show that the Cloud procedure not accounting for collapse cases strongly overestimates the median of the fragilities, especially for higher limit states such as DS3. Finally, the simplified procedure relying on the monitoring of inter-storey drifts (green curves in Figure 14) returns comparable results to the cloud methodology performed using the more detailed process of monitoring each and all connection elements.

7.3 | Connection-based fragility curves

From the results of the multiple NLTHAs, vulnerability models for low-damage connections were fitted using the Cloud methodology.

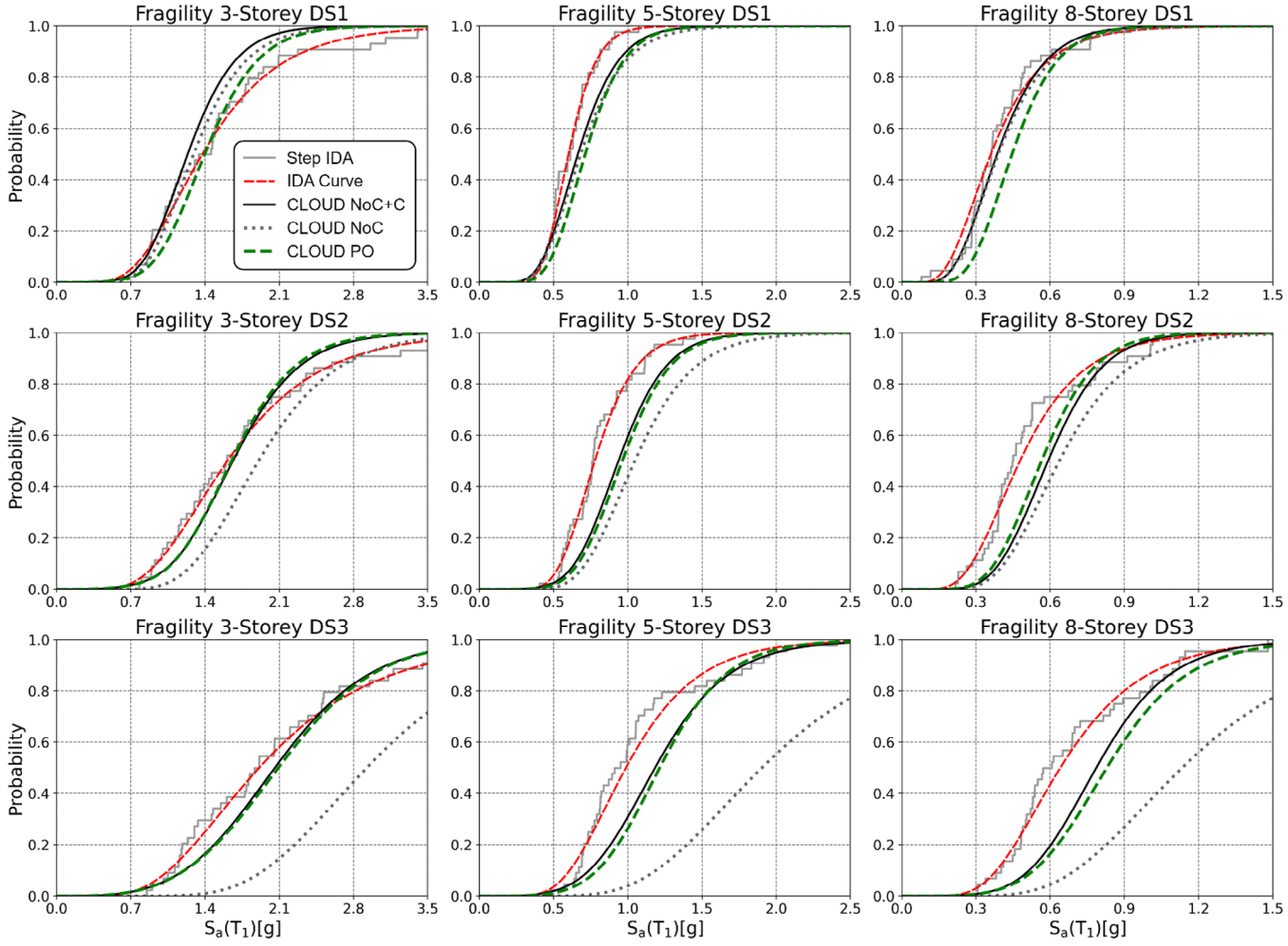

FIGURE 14 Results for global fragility curves corresponding to different damage state levels. CLOUD NoC, Cloud methodology not accounting for Collapse case; CLOUD NoC+C, Cloud methodology accounting for Collapse cases; CLOUD PO, Cloud methodology employing thresholds derived from the PushOver analysis to define the damage states thresholds in term of interstorey drift.

After conducting 141 NLTHAs using unscaled ground motions on 3 case studies for a total of 16 different internal and external beam-column connections, the complete dataset comprised a total of 2256 different datapoints for each connection type. The datapoints were then filtered to exclude cases where the NLTHA failed as well as outliers with maximum recorded inter-storey drift below 0.05% or over 10%. The final datasets were composed of approximately 2000 unique datapoints each.

The large number of different configurations enabled the definition of component-based fragility curves taking into account the component-to-component variability regarding the element section, the reinforcement details, the post-tensioning force and the location within the case-study building.

The number of recorded datapoints for column-to-foundation connections were lower compared to the beam-column connections. Consequently, a decision was made to combine internal and external connections in a single pool. The total number of unique datapoints before filtering out outliers was only 846 (423 for internal and 423 for external connections). For this reason, columns-to-foundation results presented in this paper are less reliable.

As shown in Figure 15, the data is well-fitted using a simple linear distribution on the logarithmic plane, especially for the beam-to-column connections. The results provide a dispersion value of around 0.3 showing higher dispersion for DS1 limit states and lower for DS2 and DS3. This might be related to the higher variability in the reinforcement details, such as the dissipator diameter, that strongly influence the strain capacity of external devices. Moreover, the external beam-column connections show a slightly larger dispersion value compared to the internal ones.

The reduced number of datapoints concerning the column-to-foundation interfaces leads to a low value of beta for the DS1 limit state, probably due to the low variability in the reinforcement detailing of column-to-foundation connections (as

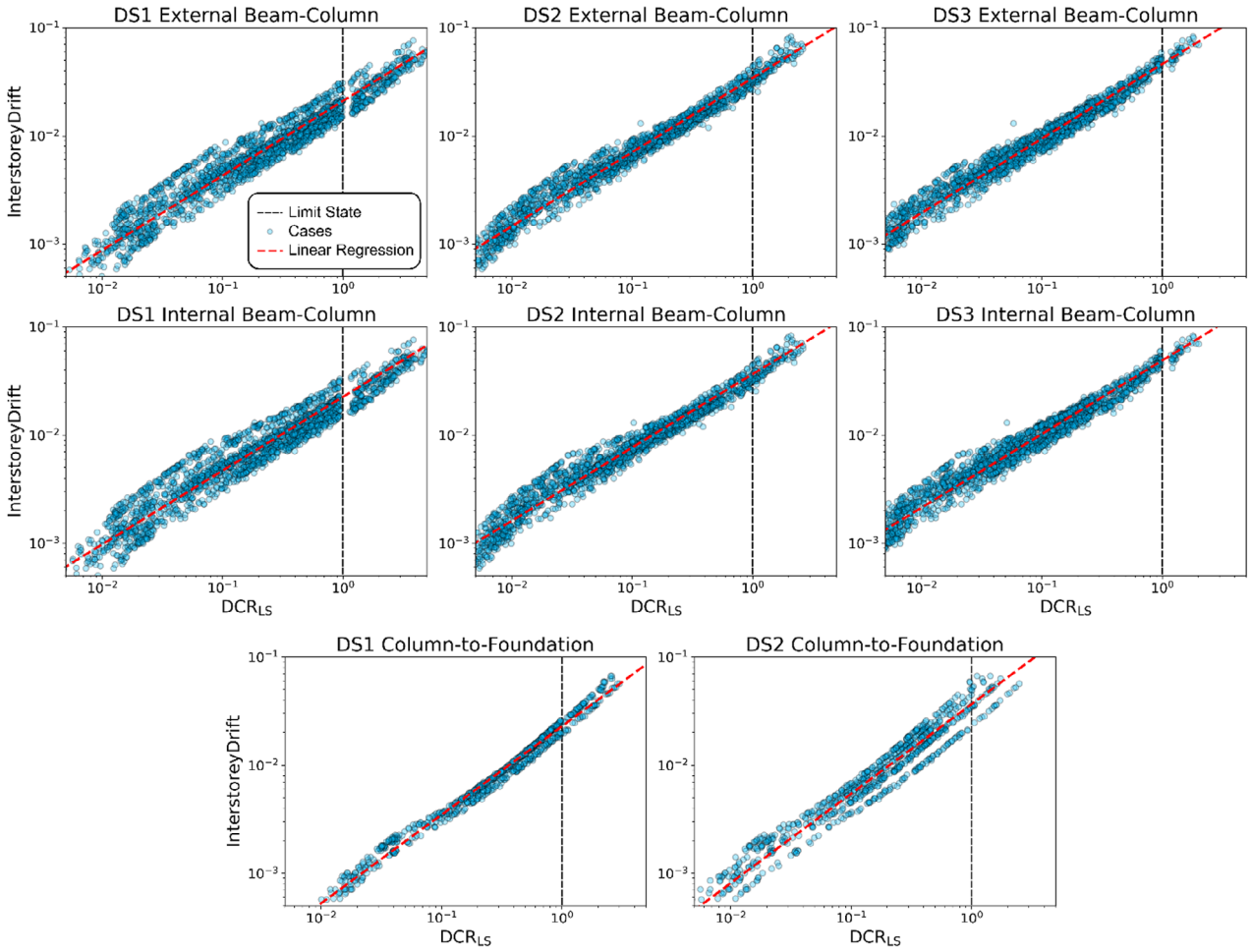

FIGURE 15 Cloud models for connection type and damage state.

reported in Table 5). Moreover, the DS2 is strongly dependent on axial load and member sizes; therefore, the data shows a larger dispersion. To better characterize the fragility of this connection, more case-studies should be analysed to increase the number of datapoints.

It is found that the median value of the fragility curve at onset of DS1 is, for all cases, slightly larger than 2%, in line with the expected drift value at Life Safety limit state. Meanwhile, the median value for the fragility at onset of DS3 is above 4%, which is the expected drift value at collapse limit state. Timber yielding on average occurs when a drift of 3% and above is reached, sitting between the life safety and collapse limit state.

The results show that external beam-to-column connections are arguably the most vulnerable connection in a Pres-Lam frame system, reaching the limit states at a lower drift value. This is due to the lower deformation of the external joint panel zones compared to the internal ones. Despite Equations 10 and 11 showing higher stiffness of internal joints, they are subject to higher stresses, resulting in higher deformations. However, it is highlighted that, despite the results give a different median value for the internal and external connections regarding DS3, this does not reflect the behaviour of such connections, being the tendon unbonded for the whole frame's length. For this reason, a more representative value can be obtained by averaging the two values weighted on the number of connection types:

$$\theta_{DS3} = \frac{(Nspans - 1)\,\theta_{DS3,int} + \theta_{DS3,ex}}{Nspans} \tag{12}$$

A more conservative approach would be to consider the lowest value between the internal and external threshold.

Fragility curves are shown in Figure 16 and their median/dispersion values are summarized in Table 9.

When focusing on the beam-column connections, it is also found that the DS1 is associated with a larger dispersion of datapoints when compared to the higher damage states. This result is related to the failure of the external dissipaters

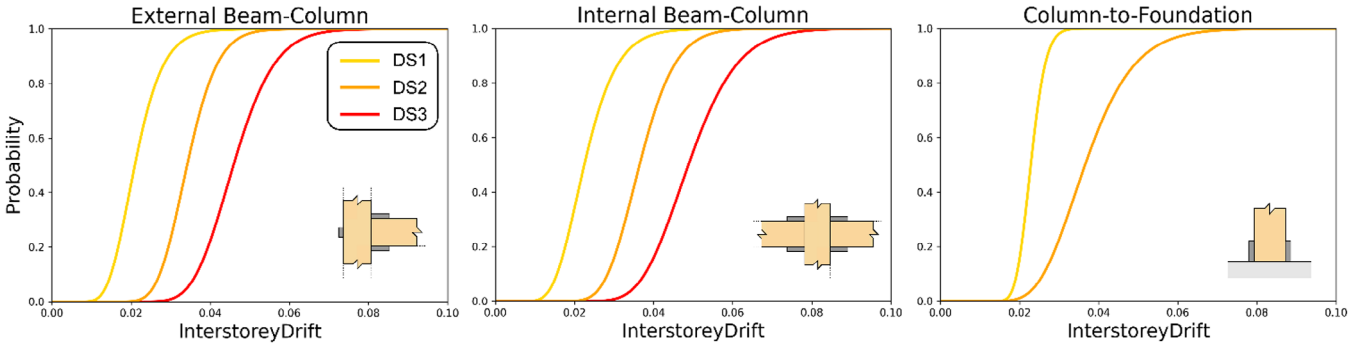

FIGURE 16 Fragility models for low-damage structural connections.

TABLE 9 Median (μ) and Beta (β) values for the fragility curves of structural connections.

	DS1		DS2		DS3	
Component	μ	β	μ	β	μ	β
External beam-column connection	2.09%	0.386	3.42%	0.258	4.59%	0.260
Internal beam-column connection	2.25%	0.419	3.65%	0.287	4.88%	0.293
Column-to-foundation connection	2.28%	0.161	3.66%	0.319	–	–

before the higher damage states, involving compression yielding of the timber and/or yielding of the unbonded tendons, are reached, leading to lower variability of possible connection configurations thus reducing the number of uncertainties related to the fragility model. However, this is not observed in the column-to-foundation connections due the lack of variations in reinforcement details.

8 | CONCLUSION

This article has proposed and validated a comprehensive framework for the estimation of fragility curves for post-tensioned (Pres-Lam) timber frames—at both system and connection levels. IDA and Cloud Methodology were implemented for defining fragility curves by means of DCRs and inter-storey drifts from static non-linear pushover analyses. The different methodologies were tested on three case-study buildings through the development of a parametric BIM-oriented model in OpenSEES and Revit. The frames were modelled using a lumped plasticity approach to simulate the behaviour of the hybrid low-damage connections, and the model was calibrated against experimental testing. The data obtained from the numerical analyses was finally used to fit fragility models for Pres-Lam hybrid connections considering the inter-storey drift as the engineering demand parameter (EDP).

Relatively to the building-level fragility functions, the main findings can be summarized as follow:

- The IDA approach usually yields more conservative results when compared to the Cloud methodology, especially for higher damage states.
- The Cloud methodology leads to a considerable overestimation of fragility functions when not considering collapse cases.
- The approach that makes use of pushover analyses to determine the drift related thresholds for the onset of limit states yields similar results to the more complex DCR approach, especially for higher damage states.

Relatively to the connection-level fragility functions, the main findings can be summarized as follow:

- The methodology was able to produce satisfactory results managing to yield fragility functions for structural connections.
- The onset of damage states for beam-column connections is expected for values of inter-storey drifts of around 2.2%, 3.5%, and 4.7% for DS1, DS2, and DS3, respectively.

- DS1 fragility functions exhibit a higher dispersion relative to DS2 and DS3 because of the increased variability related to reinforcement details, which is partially lost after the mild steel fails.
- Despite the fragility function for column-to-foundation connections where fitted, the results are still constrained by the reduced amount of data.

As further development, more effort should be directed into characterizing the fragility functions for column-to-foundation connections as well as the introduction of different sources of variability such as material uncertainties. Furthermore, consequence functions should be developed for the investigated structural connections to allow for the application of a connection -level loss assessment methodology.

ACKNOWLEDGEMENTS

Authors acknowledge the financial support for Michele Matteoni's PhD scholarship provided by the PNRR funding scheme (Piano Nazionale di Ripresa e Resilienza, in Italian) as part of the National Research Centre CN1 on "High-Performance Computing, Big Data and Quantum Computing"—Spoke 5 - Environment and Natural Disaster: Framework and methodologies for impact evaluation and risk mitigation, whose support is greatly appreciated. The authors also acknowledge the financial support from the 'ENHANCE project' grant agreement C.U.P. 'B89J21022640002', and the European Union through the Horizon Europe Research & Innovation Programme (Grant Agreement no. 101123467 MULTICARE—Multi-hazard low-carbon resilient technologies and multi-scale digital services for a future-proof, sustainable & user-centred built environment). The authors finally acknowledge the valuable support from their colleagues and fellow members of the research group, Livio Pedone, Simone D'Amore, Giada Formichetti and Alessandra Miliziano.

CONFLICT OF INTEREST STATEMENT

The author(s) declared no potential conflicts of interest concerning the research, authorship and/or publication of this article.

DATA AVAILABILITY STATEMENT

The data that support the findings of this study are available from the corresponding author upon reasonable request.

ORCID

Michele Matteoni https://orcid.org/0000-0001-7155-1449

REFERENCES

1. Galasso C, McCloskey J, Pelling M, et al. Editorial. Risk-based, Pro-poor urban design and planning for tomorrow's cities. *Int Journal of Disaster Risk Reduction*. 2021;58:102158. doi:10.1016/j.ijdrr.2021.102158
2. Pampanin S. Reality-check and renewed challenges in earthquake engineering. *Bull N Z Soc Earthquake Eng*. 2012;45(4):137-160. doi:10.5459/bnzsee.45.4.137-160
3. Whittaker A, Soong TT. An overview of nonstructural research at three U.S. Earthquake Engineering Research Centers. In: ATC-29-2 seminar on the seismic design, performance and retrofit of nonstructural components in critical facilities, Irvine, CA, USA, 2003.
4. Menna C, Asprone D, Jalayer F, Prota A, Manfredi G. Assessment of ecological sustainability of a building subjected to potential seismic events during its lifetime. *Int J Life Cycle Assess*. 2012;18(2):504-515. doi:10.1007/s11367-012-0477-9
5. Belleri A, Marini A. Does seismic risk affect the environmental impact of existing buildings. *Energy Build*. 2016;110:149-158.
6. Bianchi S, Ciurlanti J, Overend M, Pampanin S. Low-carbon & low-damage technologies for improving the resilience of buildings. Proceedings of the 2023 Society for Earthquake and Civil Engineering Dynamics Conference, Cambridge, UK, 2023.
7. GlobalABC. IEA and UNEP, 2019 global status report for buildings and construction: Towards a zeroemission, efficient and resilient buildings and construction sector, Global Alliance for Buildings and Construction, International Energy Agency and the United Nations Environment Programme, 2019.
8. Popovski M, Gavric I. Performance of a 2-story CLT house subjected to lateral loads. *J Struct Eng*. 2016;142(4). doi:10.1061/(asce)st.1943-541x.0001315
9. van de Lindt JW, Furley J, Amini MO, et al. Experimental seismic behavior of a two-story CLT platform building. *Eng Struct*. 2019;183:408-422. doi:10.1016/j.engstruct.2018.12.079
10. van de Lindt JW, Pei S, Pryor SE, Shimizu H, Isoda H. Experimental seismic response of a full-scale six-story light-frame wood building. *J Struct Eng*. 2010;136(10):1262-1272. doi:10.1061/(asce)st.1943-541x.0000222
11. Zhang X, Isoda H, Sumida K, et al. Seismic performance of three-story cross-laminated timber structures in Japan. *J Struct Eng*. 2021;147(2). doi:10.1061/(asce)st.1943-541x.0002897

12. Aloisio A, Fragiacomo M. Reliability-based overstrength factors of cross-laminated timber shear walls for seismic design. *Eng Struct*. 2021;228:111547. doi:10.1016/j.engstruct.2020.111547
13. Palermo A, Pampanin S, Buchanan A, Newcombe MP. *Seismic Design of Multi-storey Buildings using Laminated Veneer Lumber (LVL)*. New Zealand Society for Earthquake Engineering Conference; 2005.
14. Pampanin S, Palermo A, Buchanan A, Fragiacomo M, Deam BL. Code Provisions for Seismic Design of Multi-storey Post-tensioned Timber Buildings. 39th Meeting of the Working Commission W18-Timber Structures, CIB, International Council for Research and Innovation, Florence, Italy, 2006.
15. Granello G, Palermo A, Pampanin S, Pei S, van de Lindt J. Pres-Lam buildings: state-of-the-art. *J Struct Eng*. 2020;146(6). doi:10.1061/(asce)st.1943-541x.0002603
16. Priestley MJN. Overview of PRESSS Research Program. *PCI Journal*. 1991;36(4):50-57. 10.15554/pcij.07011991.50.57
17. Stanton J, Stone WC, Cheok GS. A hybrid reinforced precast frame for seismic regions. *PCI Journal*. 1997;42(2):20-23. 10.15554/pcij.03011997.20.23
18. Priestley MJN, Sritharan S, Conley JR, Stefano Pampanin S. Preliminary results and conclusions from the PRESSS five-story precast concrete test building. *PCI Journal*. 1999;44(6):42-67. 10.15554/pcij.11011999.42.67
19. Pampanin S. Emerging solutions for high seismic performance of precast/prestressed concrete buildings. *J Adv Concr Technol*. 2005;3(2):207-223. doi:10.3151/jact.3.207
20. Johnston H, Watson C, Pampanin S. Shake table testing of an integrated low damage building system. Second European Conference on Earthquake Engineering and Seismology, Istanbul, Turkey, 2014.
21. Marriott D, Pampanin S, Bull D, Palermo A. Dynamic testing of precast, post-tensioned rocking wall systems with alternative dissipating solutions. *Bull N Z Soc Earthquake Eng*. 2008;41(2):90-103. doi:10.5459/bnzsee.41.2.90-103
22. Sarti F, Palermo A, Pampanin S. Fuse-type external replaceable dissipaters: experimental program and numerical modeling. *J Struct Eng*. 2016;142(12). doi:10.1061/(asce)st.1943-541x.0001606
23. Christopoulos C, Filiatrault A, Uang CM, Folz B. Posttensioned energy dissipating connections for moment-resisting steel frames. *J Struct Eng*. 2002;128(9):1111-1120. doi:10.1061/(asce)0733-9445(2002)128:9(1111)
24. Filiatrault A, Sullivan T. Performance-based seismic design of nonstructural building components: the next frontier of earthquake engineering. *Earthquake Eng Engineering Vibr*. 2014;13(S1):17-46. doi:10.1007/s11803-014-0238-9
25. Pampanin S. Towards the "Ultimate Earthquake-Proof" Building: development of an integrated low-damage system. *Perspect Eur Earthquake Eng Seismol*. 2015:321-358. doi:10.1007/978-3-319-16964-4_13
26. D'Amore S, Bianchi S, Ciurlanti J, Pampanin S. Seismic assessment and finite element modeling of traditional vs innovative point fixed glass facade systems (PFGFS). *Bull Earthquake Eng*. 2023;21(5):2657-2689. doi:10.1007/s10518-023-01622-0
27. Pampanin S, Ciurlanti J, Bianchi S, et al. Triaxial shake table testing of an integrated low-damage building system. *Earthquake Eng Struct Dyn*. 2023;52(10):2983-3007. doi:10.1002/eqe.3906
28. Ciurlanti J, Bianchi S, Pampanin S. Raising the bar in seismic design: cost–benefit analysis of alternative design methodologies and earthquake-resistant technologies. *Bull Earthquake Eng*. 2023;21(5):2723-2757. doi:10.1007/s10518-023-01625-x
29. Palermo A, Pampanin S, Buchanan A, Experimental investigations on LVL seismic resistant wall and frame subassemblies. Proceedings of the 1st European Conference on Earthquake Engineering and Seismology, Geneva, Italy, 2006.
30. Iqbal A, Pampanin S, Buchanan AH, Palermo A. Improved seismic performance of LVL post-tensioned walls coupled with UFP devices. Proceedings of 8th Pacific Conference on Earthquake Engineering, Singapore, 2007.
31. Newcombe MP, Pampanin S, Buchanan A, Palermo A. Section analysis and cyclic behavior of post-tensioned jointed ductile connections for multi-story timber buildings. *J Earthquake Eng*. 2008;12(1):83-110. doi:10.1080/13632460801925632
32. Iqbal A, Pampanin S, Palermo A. Seismic performance of prestressed timber beam column sub-assemblies. Proc. of annual conference of New Zealand society for earthquake engineering, Wellington, New Zealand, 2010.
33. Wanninger F, Frangi A. Experimental and analytical analysis of a post-tensioned timber connection under gravity loads. *Eng Struct*. 2014;70:117-129. doi:10.1016/j.engstruct.2014.03.042
34. Sarti F, Palermo A, Pampanin S. Quasi-static cyclic testing of two-thirds scale unbonded posttensioned rocking dissipative timber walls. *J Struct Eng*. 2016;142(4). doi:10.1061/(asce)st.1943-541x.0001291
35. Moroder D, Smith T, Dunbar A, Pampanin S, Buchanan A. Seismic testing of post-tensioned Pres-Lam core walls using cross laminated timber. *Eng Struct*. 2018;167:639-654. doi:10.1016/j.engstruct.2018.02.075
36. Newcombe MP, Pampanin S, Buchanan A. *Global response of a two-storey Pres-Lam building*. New Zealand Society for Earthquake Engineering Conference; 2010.
37. Brown A, Lester J, Pampanin S, Pietra D. Pres-Lam in practice—a damage-limiting rebuild project. Structural Engineering Society SESOC New Zealand Conference, Auckland, New Zealand, 2012.
38. Curtain B, Dekker D, Chung S, Palermo A. Design of Carterton Event Centre: an example of innovative collaboration between architecture and timber engineering. Proceedings of the 12th world conference on timber engineering WCTE, Auckland, New Zealand, 2012.
39. Leyder C, Wanninger F, Frangi A, Chatzi E. Dynamic response of an innovative hybrid structure in hardwood. *Proc Inst Civil Eng Construct Mater*. 2015;168(3):132-143. doi:10.1680/coma.14.00043
40. Holden T, Devereux C, Haydon S, Buchanan A, Pampanin S. NMIT Arts & Media Building—Innovative structural design of a three storey post-tensioned timber building. *Case Studies Struct Eng*. 2016;6:76-83. doi:10.1016/j.csse.2016.06.003

41. Sarti F, Palermo A, Pampanin S, Berman J. Determination of the seismic performance factors for post-tensioned rocking timber wall systems. *Earthquake Eng Struct Dyn*. 2017;46(2):181-200. doi:10.1002/eqe.2784
42. Pampanin S, Ciurlanti J, Bianchi S. Overview of SERA Project: 3D shaking table tests on an integrated low-damage building system. Proceedings of 4SPONSE Workshop 2019. doi:10.7414/4sponse.ID.60
43. Miliziano A, Granello G, Palermo A, Pampanin S. Overview of connection detailing for post-tensioned dissipative timber frames. *Struct Eng Int*. 2020;30(2):209-216. doi:10.1080/10168664.2020.1736968
44. Bianchi S, Ciurlanti J, Perrone D, et al. Shake-table tests of innovative drift sensitive nonstructural elements in a low-damage structural system. *Earthquake Eng Struct Dyn*. 2021;50(9):2398-2420. doi:10.1002/eqe.3452
45. Sarti F, Palermo A, Pampanin S, Berman J. Evaluation of the seismic performance factors of post-tensioned timber wall systems. Second European Conference on Earthquake Engineering and Seismology, Istanbul, Turkey, 2014.
46. Kovacs MA, Wiebe L. Controlled rocking CLT walls for buildings in regions of moderate seismicity: design procedure and numerical collapse assessment. *J Earthquake Eng*. 2017;23(5):750-770. doi:10.1080/13632469.2017.1326421
47. Sun X, He M, Li Z, Lam F. Seismic performance of energy-dissipating post-tensioned CLT shear wall structures II: dynamic analysis and dissipater comparison. *Soil Dyn Earthquake Eng*. 2020;130:105980. doi:10.1016/j.soildyn.2019.105980
48. Wilson AW, Phillips AR, Motter CJ, Lee JY, Dolan JD. Seismic loss analysis of buildings with post-tensioned cross-laminated timber walls. *Earthquake Spectra*. 2020;37(1):324-345. doi:10.1177/8755293020944188
49. Aloisio A, Rosso MM, Huang D, Iqbal A, Fragiacomo M, Pei S. Nonlinear analytical modeling of mass-timber buildings with post-tensioned rocking walls. *Bull Earthquake Eng*. 2022;21(1):473-502. doi:10.1007/s10518-022-01553-2
50. Granello G, Broccardo M, Palermo A, Pampanin S. Fragility-based methodology for evaluating the time-dependent seismic performance of post-tensioned timber frames. *Earthquake Spectra*. 2020;36(1):322-352. doi:10.1177/8755293019878196
51. Shinozuka M, Feng MQ, Kim HK, Kim SH. Nonlinear static procedure for fragility curve development. *J Eng Mech*. 2000;126(12):1287-1295. doi:10.1061/(asce)0733-9399(2000)126:12(1287)
52. Baker JW. Efficient analytical fragility function fitting using dynamic structural analysis. *Earthquake Spectra*. 2015;31(1):579-599. doi:10.1193/021113eqs025m
53. Cornell CA, Jalayer F, Hamburger RO, Foutch DA. Probabilistic basis for 2000 SAC Federal Emergency Management Agency Steel Moment Frame Guidelines. *J Struct Eng*. 2002;128(4):526-533. doi:10.1061/(asce)0733-9445(2002)128:4(526)
54. Vamvatsikos D, Cornell CA. Incremental dynamic analysis. *Earthquake Eng Struct Dyn*. 2002;31(3):491-514. doi:10.1002/eqe.141
55. Vamvatsikos D. Performing incremental dynamic analysis in parallel. *Comput Struct*. 2011;89(1–2):170-180. doi:10.1016/j.compstruc.2010.08.014
56. Bazzurro P, Cornell CA, Shome N, Carballo JE. Three proposals for characterizing MDOF nonlinear seismic response. *J Struct Eng*. 1998;124(11):1281-1289. doi:10.1061/(asce)0733-9445(1998)124:11(1281)
57. Baker JW. Probabilistic structural response assessment using vector-valued intensity measures. *Earthquake Eng Struct Dyn*. 2007;36(13):1861-1883. doi:10.1002/eqe.700
58. Jalayer F. *Direct Probabilistic Seismic Analysis: Implementing Non-linear Dynamic Assessments*. Ph.D. Thesis, Stanford University; 2003.
59. Jalayer F, Elefante L, Iervolino I, Manfredi G. Knowledge-based performance assessment of existing RC buildings. *J Earthquake Eng*. 2011;15(3):362-389. doi:10.1080/13632469.2010.501193
60. Jalayer F, De Risi R, Manfredi G. Bayesian Cloud analysis: efficient structural fragility assessment using linear regression. *Bull Earthquake Eng*. 2015;13(4):1183-1203. doi:10.1007/s10518-014-9692-z
61. Jalayer F, Ebrahimian H, Miano A, Manfredi G, Sezen H. Analytical fragility assessment using unscaled ground motion records. *Earthquake Eng Struct Dyn*. 2017;46(15):2639-2663. doi:10.1002/eqe.2922
62. McKenna F. OpenSees: a framework for earthquake engineering simulation. *Comput Sci Eng*. 2011;13(4):58-66. doi:10.1109/mcse.2011.66
63. Zhu M, McKenna F, Scott MH. OpenSeesPy: python library for the OpenSees finite element framework. *SoftwareX*. 2018;7:6-11. doi:10.1016/j.softx.2017.10.009
64. Federal Emergency Management Agency. Seismic performance assessment of buildings, volume 1—Methodology. Technical report FEMA-P-58-1, Department of Homeland Security, Washington, DC; 2012.
65. Bianchi S, Ciurlanti J, Pampanin S. Comparison of traditional vs low-damage structural and non-structural building systems through a cost/performance-based evaluation. *Earthquake Spectra*. 2021;37(1):366-385. doi:10.1177/8755293020952445
66. Pampanin S, Palermo A, Buchanan AH. *Design Guide Australia and New Zealand: post-Tensioned Timber Buildings-EXPAN Design Guides*. *Structural Timber Innovation Company*; 2013.
67. NTC 2018. Ministero delle Infrastrutture. Aggiornamento delle Norme Tecniche per le Costruzioni, Supplemento ordinario n°8 alle G.U.n°42 del 20/02/2018, serie generale (in Italian), Rome, Italy, 2018.
68. Lukaszewska E, Fragiacomo M, Johnsson H. Laboratory tests and numerical analyses of prefabricated timber-concrete composite floors. *J Struct Eng*. 2010;136(1):46-55. doi:10.1061/(asce)st.1943-541x.0000080
69. Newcombe MP, van Beerschoten WA, Carradine D, Pampanin S, Buchanan AH. In-plane experimental testing of timber-concrete composite floor diaphragms. *J Struct Eng*. 2010;136(11):1461-1468. doi:10.1061/(ASCE)ST.1943-541X.0000239
70. Priestley MJN. Direct displacement-based design of precast/prestressed concrete buildings. *PCI J*. 2002;47(6):66-79. 10.15554/pcij.11012002.66.79
71. Priestley MN, Calvi GM, Kowalsky MJ. *Direct Displacement-Based Seismic Design of Structures*. IUSS Press; 2007.
72. Pampanin S, Marriott D, Palermo A. *PRESSS Design Handbook*. New Zealand Concrete Society; 2010.

73. Miliziano A, Granello G, Palermo A, Pampanin S. Performance based design for post-tensioned timber frames. Proceedings of the 2019 Society for Earthquake and Civil Engineering Dynamics Conference, Greenwich, London, UK, 2019.
74. Granello G, Leyder C, Palermo A, Frangi A, Pampanin S. Design approach to predict post-tensioning losses in post-tensioned timber frames. *J Struct Eng*. 2018;144(8). doi:10.1061/(asce)st.1943-541x.0002101
75. Smith T, Ponzo FC, Di Cesare A, et al. Seismic performance of a post-tensioned glue laminated beam to column joint: experimental and numerical results. In Proceedings of the World Conference on Timber Engineering, Auckland, New Zealand, 2012.
76. Smith T, Pampanin S, Simonetti M, Di Cesare A, Ponzo FC, Nigro D. Dynamic testing of a three-storey Pres-Lam Frame. Proceedings of the Tenth Pacific Conference on Earthquake Engineering, Sydney, Australia, 2015.
77. Ponzo FC, Di Cesare A, Lamarucciola N, Nigro D, Pampanin S. Modelling of post-tensioned timber-framed buildings with seismic rocking mechanism at the column-foundation connections. *Int J Comput Methods Exp Measure*. 2017;5(6):966-978. doi:10.2495/cmem-v5-n6-966-978
78. Pampanin S, Priestley NMJ, Sritharan S. Analytical modelling of the seismic behaviour of precast concrete frames designed with ductile connections. *J Earthquake Eng*. 2001;5(3):329-367. doi:10.1080/13632460109350397
79. Palermo A. *The Use of Controlled Rocking in the Seismic Design of Bridges*. Ph.D. Thesis. Technical Institute of Milan; 2004.
80. Smith T. *Post-tensioned Timber Frames with Supplemental Damping Devices*. Ph.D. Thesis. University of Canterbury; 2014.
81. Di Cesare A, Ponzo FC, Nigro D, Pampanin S, Smith T. Shaking table testing of post-tensioned timber frame building with passive energy dissipation systems. *Bull Earthquake Eng*. 2017;15(10):4475-4498. doi:10.1007/s10518-017-0115-9
82. Federal Emergency Management Agency. Quantification of Building Seismic Performance Factors. Report No. FEMA-P695, Department of Homeland Security, Washington, DC, USA; 2008.
83. Ancheta TD, Darragh RB, Stewart JP, et al. NGA-West2 Database. *Earthquake Spectra*. 2014;30(3):989-1005. doi:10.1193/070913eqs197m
84. Jalayer F, Ebrahimian H, Miano A. Record-to-record variability and code-compatible seismic safety-checking with limited number of records. *Bull Earthquake Eng*. 2021;19(15):6361-6396. doi:10.1007/s10518-020-01024-6

How to cite this article: Matteoni M, Ciurlanti J, Bianchi S, Pampanin S. Fragility functions for low-damage post-tensioned timber frames. *Earthquake Engng Struct Dyn*. 2024;1-22. https://doi.org/10.1002/eqe.4242